JCTC Journal of Chemical Theory and Computation

Article

pubs.acs.org/JCTC

Analysis of Excitonic and Charge Transfer Interactions from Quantum Chemical Calculations

Felix Plasser*,† and Hans Lischka*,†,‡

†Institute for Theoretical Chemistry, University of Vienna, Waehringerstrasse 17, A 1090 Vienna, Austria

‡Department of Chemistry and Biochemistry, Texas Tech University, Lubbock, Texas 79409-1061, United States

Supporting Information

ABSTRACT: A procedure for a detailed analysis of excited states in systems of interacting chromophores is proposed. By considering the one-electron transition density matrix, a wealth of information is recovered that may be missed by manually analyzing the wave function. Not only are the position and spatial extent given, but insight into the intrinsic structure of the exciton is readily obtained as well. For example, the method can differentiate between excitonic and charge resonance interactions even in completely symmetric systems. Four examples are considered to highlight the utility of the approach: interactions between the nπ^* states in a formaldehyde dimer, excimer formation in the naphthalene dimer, stacking interaction in an adenine dimer, and the excitonic band structure in a conjugated phenylenevinylene oligomer.

1. INTRODUCTION

Excited states in multichromophoric systems have recently gained a substantial amount of interest. One example is DNA, where interactions between nucleobases have been shown to significantly alter the excited-state behavior as compared to that of its isolated constitutents.[1,2] In particular, the amount of delocalization and the question of whether the resulting states are of excitonic or charge transfer nature and how interconversions could happen have been discussed intensively.[3−7] Another area that has been gaining significant attention is organic electronics. There it is of particular interest to analyze the spatial extent of an exciton and the average electron hole separation and to understand the processes of charge separation and recombination.[8−11] Both cases are examples where a detailed description of the structure of the exciton is decisive for understanding the processes and where a simple visual analysis of the large number of contributing molecular orbitals and configurations is not only cumbersome but may miss important information. Furthermore, if statistical data are needed, it is important to have well-defined quantities which are easily used in an automated analysis. In this paper we will present a strategy for detailed analysis of quantum chemical excited-state calculations in dimers, oligomers, and extended systems, which allows drawing a direct relation to physical models.

Our approach is based on an analysis of the one-electron transition density matrices between the ground and electronically excited states. It provides a direct and straightforward procedure to characterize the aforementioned excitonic and charge transfer processes. Related work by Luzanov[12,13] provides a firm mathematical background. Tretiak and Mukamel have formulated a similar analysis specifically for conjugated polymers.[8] As a complementary approach, a singular value decomposition of the transition density matrix to obtain the natural transition orbitals has been applied by several authors as well.[14−16] In contrast to our methods, also the one-electron difference density matrix has been used to describe electronic transitions.[17] Thus, many of the underlying concepts are already known. However, we believe that, building on the above-mentioned work, we can provide a significant amount of new applicability by connecting the different ideas, by providing compact automatized descriptors, and by supplying a programming interface that may be easily extended to many different wave function models and quantum chemistry programs.

In this work the basic procedures and the final formalism will be presented, followed by representative examples which should demonstrate the power and the usefulness of our methods. First, the stacked formaldehyde dimer will be explored, followed by an analysis of excimer formation in the naphthalene dimer. Especially the second example will illustrate the strength of our analysis as compared to the quite involved direct analysis of the electronic wave function. Finally, the analysis of two systems of highest current interest, a diadenine stack in B-DNA geometry and a phenylenevinylene oligomer, will be presented.

2. METHODOLOGY

If two or more chromophores come into contact, not only do interactions between the excited states on each chromophore have to be considered, but also charge transfer states come into play. For example, in a dimer there are four states per type of monomer transition: a local excitation on each fragment and two charge transfer states going in either direction (Figure 1).[18] At small intermolecular separations (<5 Å in π-systems[18]) all four states may interact, yielding eigenfunctions which can be arbitrary mixtures of these states.[19] The situation becomes more complex if more than two chromophores are involved because a large number of possible local and charge transfer transitions have to be considered. Below, an approach is described for analyzing excited states obtained in quantum

Received: April 16, 2012
Published: June 21, 2012

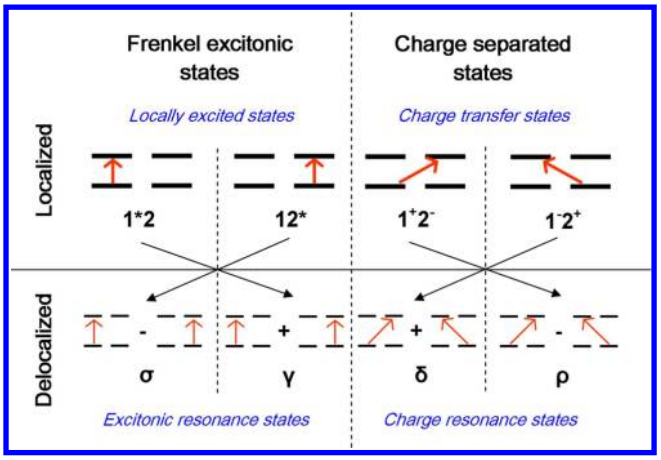

Figure 1. Depiction of dimer excited states arising from one type of transition in the monomer. Localized excited states (top) and their linear combinations leading to delocalized states (bottom) are shown.

chemical computations, which allows reconstructing such contributions systematically. First, the concepts of interest will be briefly illustrated by using a dimer of interacting chromophores. Second, on the basis of these considerations, the charge transfer numbers,[12,13] a general measure for decomposing an exciton into locally excited and charge transfer contributions, will be considered. Furthermore, strategies for reducing this information in systems with a larger number of chromophores will be discussed. Finally, it will be outlined how natural transition orbitals[14−16] may be used to define an intrinsic measure for resonant delocalization (see also ref 20).

The nomenclature used in the following text is outlined in Figure 1. The term "Frenkel exciton" refers to excited states where for every transition the *initial* and *final* orbitals are located on the same respective fragment. These may be "locally excited states" with only one fragment involved or "excitonic resonance states" if two or more fragments are involved. Contrary to Frenkel excitons, the term "charge-separated states" refers to states where for every transition the initial and final orbitals are located on different fragments. Such states may exhibit a net transfer of charge, resulting in a "charge transfer state". Alternatively, two opposing charge transfer transitions may come into resonance, producing a charge resonance state without net transfer of charge. In the following discussion these four limiting cases will be considered. In practice, also mixtures between these types are possible.

In this context it may be noted that by consideration of summed attachment and detachment densities,[17] which is a complementary way to represent an excitation, it would not be possible to differentiate between excitonic resonance and charge resonance states (Figure 1, bottom): both kinds of states would yield evenly delocalized attachment and detachment densities.

2.1. Introductory Example. To illustrate the concepts involved, first the standard model for excited states on two interacting molecules will be briefly reviewed.[18,19] Two molecules, "1" and "2", are considered, each with two active orbitals, forming an orthonormal set of four orbitals: i (initial) and f (final) on fragment 1, i′ and f′ on fragment 2. The initial orbitals are doubly occupied in the ground state, whereas the final orbitals are unoccupied. Considering these orbitals, it is possible to construct four states by single excitations from a Hartree−Fock ground state $|0\rangle$ (cf. Figure 1, top). Using spin-averaged excitation operators (cf., for example, ref 21), these may be written in a compact form as

$$|1^*2\rangle = 2^{-1/2}E_{\mathrm{fi}}|0\rangle \tag{1}$$

$$|12^*\rangle = 2^{-1/2}E_{\mathrm{f'i'}}|0\rangle \tag{2}$$

$$|1^-2^+\rangle = 2^{-1/2}E_{\mathrm{fi'}}|0\rangle \tag{3}$$

$$|1^+2^-\rangle = 2^{-1/2}E_{\mathrm{f'i}}|0\rangle \tag{4}$$

where E_{rs} denotes the excitation from orbital s to orbital r (consider ref 18 for the explicit expressions of these states). The first two states correspond to locally excited states. The remaining two are charge-separated states with a net transfer of a unit charge.

In the presence of symmetry, the states $|1^*2\rangle$ and $|12^*\rangle$ as well as $|1^-2^+\rangle$ and $|1^+2^-\rangle$ are pairwise degenerate, yielding delocalized eigenfunctions. At large intermolecular separations, these can be clearly divided into two types (cf. Figure 1, bottom): Frenkel excitonic resonance states (where excitations always occur within one fragment)

$$\begin{aligned}|\sigma\rangle &= \frac{1}{\sqrt{2}}(|1^*2\rangle - |12^*\rangle)\\ &= \frac{1}{2}(E_{\mathrm{fi}} - E_{\mathrm{f'i'}})|0\\ &= \frac{1}{2}(E_{\mathrm{f^+i^-}} + E_{\mathrm{f^-i^+}})|0\rangle\end{aligned} \tag{5}$$

$$\begin{aligned}|\gamma\rangle &= \frac{1}{\sqrt{2}}(|1^*2\rangle + |12^*\rangle)\\ &= \frac{1}{2}(E_{\mathrm{fi}} + E_{\mathrm{f'i'}})|0\rangle\\ &= \frac{1}{2}(E_{\mathrm{f^-i^-}} + E_{\mathrm{f^+i^+}})|0\rangle\end{aligned} \tag{6}$$

and charge resonance states (where excitations always go across fragments)

$$\begin{aligned}|\delta\rangle &= \frac{1}{\sqrt{2}}(|1^-2^+\rangle + |1^+2^-\rangle)\\ &= \frac{1}{2}(E_{\mathrm{fi'}} + E_{\mathrm{f'i}})|0\rangle\\ &= \frac{1}{2}(E_{\mathrm{f^-i^-}} - E_{\mathrm{f^+i^+}})|0\rangle\end{aligned} \tag{7}$$

$$\begin{aligned}|\rho\rangle &= \frac{1}{\sqrt{2}}(|1^-2^+\rangle - |1^+2^-\rangle)\\ &= \frac{1}{2}(E_{\mathrm{fi'}} - E_{\mathrm{f'i}})|0\rangle\\ &= \frac{1}{2}(E_{\mathrm{f^+i^-}} - E_{\mathrm{f^-i^+}})|0\rangle\end{aligned} \tag{8}$$

The states are given here in the localized basis, as well as in the basis of delocalized orbitals defined as $\mathrm{i}^+ = 2^{-1/2}(\mathrm{i} + \mathrm{i}')$, $\mathrm{i}^- = 2^{-1/2}(\mathrm{i} - \mathrm{i}')$, $\mathrm{f}^+ = 2^{-1/2}(\mathrm{f} + \mathrm{f}')$, and $\mathrm{f}^- = 2^{-1/2}(\mathrm{f} - \mathrm{f}')$; cf. ref 18. It can be seen that a differentiation between $|\sigma\rangle$ and $|\rho\rangle$ or $|\gamma\rangle$ and $|\delta\rangle$ is easily accomplished in the localized basis but quite challenging when delocalized orbitals are present, considering that they consist of the same pair of configurations and only the relative sign differentiates between them.

An interesting observation is that a single excitation between delocalized orbitals, e.g.

$$|\chi^{-/+}\rangle = 2^{-1/2}E_{f^+i^-}|0\rangle = 2^{-3/2}(E_{f\hat{i}} - E_{\hat{f}i'} + E_{f'i} + E_{f'i'})|0\rangle \quad (9)$$

yields an even mixture of locally excited and charge transfer contributions when written in the localized basis. Considering this, it is only possible to have a pure delocalized Frenkel excitonic or charge resonance state when at least two configurations (and four orbitals) are involved in the manner described above. This property will be discussed in more detail in section 2.4.

In general, it is also possible to represent localized states (or directed charge transfer states) in terms of delocalized orbitals, e.g.

$$|1^*2\rangle = 2^{-3/2}(E_{f^+i^-} + E_{f^-i^+} + E_{f^-i^-} + E_{f^+i^+})|0\rangle \quad (10)$$

which is even more difficult to understand by a quick inspection. It is therefore apparent that a rigorous analysis method may be of great benefit.

For an analysis of these states, the one-electron transition density matrix with respect to the ground state will be used; cf. refs 8, 12, and 13. It is defined for an excited state α as

$$D_{rs}^{0\alpha} = \langle 0|E_{rs}|\alpha\rangle \quad (11)$$

where r and s are two orbital indices. With a single determinant ground state, the transition density matrix simply corresponds to the one-electron excitation operators applied when constructing the excited state. The transition densities obtained in this way for the four localized states (Figure 1, top) are shown in Table 1. The crucial point here is that locally excited states are represented in the diagonal blocks corresponding to the particular fragment, whereas the charge transfer states correspond to off-diagonal blocks. For the delocalized states (Figure 1, bottom) the transition densities (expressed in localized orbitals) are shown in Table 2. It can be seen that the Frenkel excitonic states $|\sigma\rangle$ and $|\gamma\rangle$ are represented on the diagonal blocks. In contrast, the charge resonance states $|\delta\rangle$ and $|\rho\rangle$ have nonvanishing elements only in the off-diagonal blocks.

Table 1. Transition Density Matrices ($\mathbf{D}^{0\alpha}$) Represented in the Localized Orbital Basis Arranged According to (i,f,i′,f′), Charge Transfer Number Matrices $\mathbf{\Omega}^{0\alpha}$,[a] and Descriptors CT, PR, POS,[b] and PR_{NTO}[c] of Idealized Locally Excited States $|1^*2\rangle$ and $|12^*\rangle$ and Charge Transfer States $|1^-2^+\rangle$ and $|1^+2^-\rangle$ in a Dimer of Interacting Molecules

state	$\|1^*2\rangle$	$\|12^*\rangle$	$\|1^-2^+\rangle$	$\|1^+2^-\rangle$
$\mathbf{D}^{0\alpha}$	$\begin{bmatrix}0 & \sqrt{2} & 0 & 0\\ 0 & 0 & 0 & 0\\ 0 & 0 & 0 & 0\\ 0 & 0 & 0 & 0\end{bmatrix}$	$\begin{bmatrix}0 & 0 & 0 & 0\\ 0 & 0 & 0 & 0\\ 0 & 0 & 0 & \sqrt{2}\\ 0 & 0 & 0 & 0\end{bmatrix}$	$\begin{bmatrix}0 & 0 & 0 & 0\\ 0 & 0 & 0 & 0\\ 0 & \sqrt{2} & 0 & 0\\ 0 & 0 & 0 & 0\end{bmatrix}$	$\begin{bmatrix}0 & 0 & \sqrt{2} & 0\\ 0 & 0 & 0 & 0\\ 0 & 0 & 0 & 0\\ 0 & 0 & 0 & 0\end{bmatrix}$
$\mathbf{\Omega}^{0\alpha}$	$\begin{bmatrix}1 & 0\\ 0 & 0\end{bmatrix}$	$\begin{bmatrix}0 & 0\\ 0 & 1\end{bmatrix}$	$\begin{bmatrix}0 & 0\\ 1 & 0\end{bmatrix}$	$\begin{bmatrix}0 & 1\\ 0 & 0\end{bmatrix}$
CT	0	0	1	1
PR	1	1	1	1
POS	1	2	1.5	1.5
PR_{NTO}	1	1	1	1

[a]Defined in section 2.2. [b]Defined in section 2.3. [c]Defined in section 2.4.

Table 2. Transition Density Matrices ($\mathbf{D}^{0\alpha}$) Represented in the Localized Orbital Basis Arranged According to (i,f,i′,f′), Charge Transfer Number Matrices $\mathbf{\Omega}^{0\alpha}$,[a] and Descriptors CT, PR, POS,[b] and PR_{NTO}[c] of Idealized Frenkel Excitonic Resonance States σ and γ as Well as Charge Resonance States δ and ρ in a Dimer of Interacting Molecules

state	σ	γ	δ	ρ
$\mathbf{D}^{0\alpha}$	$\begin{bmatrix}0 & 1 & 0 & 0\\ 0 & 0 & 0 & 0\\ 0 & 0 & 0 & -1\\ 0 & 0 & 0 & 0\end{bmatrix}$	$\begin{bmatrix}0 & 1 & 0 & 0\\ 0 & 0 & 0 & 0\\ 0 & 0 & 0 & 1\\ 0 & 0 & 0 & 0\end{bmatrix}$	$\begin{bmatrix}0 & 0 & 1 & 0\\ 0 & 0 & 0 & 0\\ 0 & 1 & 0 & 0\\ 0 & 0 & 0 & 0\end{bmatrix}$	$\begin{bmatrix}0 & 0 & 1 & 0\\ 0 & 0 & 0 & 0\\ 0 & -1 & 0 & 0\\ 0 & 0 & 0 & 0\end{bmatrix}$
$\mathbf{\Omega}^{0\alpha}$	$\begin{bmatrix}0.5 & 0\\ 0 & 0.5\end{bmatrix}$	$\begin{bmatrix}0.5 & 0\\ 0 & 0.5\end{bmatrix}$	$\begin{bmatrix}0 & 0.5\\ 0.5 & 0\end{bmatrix}$	$\begin{bmatrix}0 & 0.5\\ 0.5 & 0\end{bmatrix}$
CT	0	0	1	1
PR	2	2	2	2
POS	1.5	1.5	1.5	1.5
PR_{NTO}	2	2	2	2

[a]Defined in section 2.2. [b]Defined in section 2.3. [c]Defined in section 2.4.

2.2. Charge Transfer Numbers. Following the above considerations, the one-electron transition density matrix may be seen as a central quantity recovering the excitations leading to a one-electron excited state; cf. refs 8, 12, and 13. If a basis of orthogonal localized orbitals were available, the following procedure could be envisaged: An element $D_{ab}^{0\alpha,[LO]}$ of the transition density matrix in this localized basis (the first part of the superscript refers to the transition from the ground state to state α, the second part to the orbital basis) corresponds to a local excitation on a fragment A if orbitals a and b are both situated on A and to a charge transfer excitation if a and b are on different fragments. A charge transfer number[12] Ω_{AB}^{α} could simply be defined by summing over all contributions on the respective fragments:

$$\Omega_{AB}^{\alpha} = \frac{1}{2}\sum_{\substack{a\in A\\ b\in B}} (D_{ab}^{0\alpha,[LO]})^2 \quad (12)$$

If A ≠ B, this represents the weight of an A → B charge transfer, and $\hat{\Omega}_{AA}^{\alpha}$ is the weight of local excitations on A. Luzanov has shown that this has in fact properties of a two-particle quantity, describing correlations between the *electron* and *hole* positions,[13] which is crucial, for example, for differentiating between Frenkel excitonic and charge resonance states (cf. Figure 1). The charge transfer numbers of the four localized dimer states (Figure 1, top) are presented in Table 1. These states can be clearly differentiated, as each state has one unique nonvanishing element of its $\mathbf{\Omega}^{\alpha}$ matrix. For the resonant delocalized states (Figure 1, bottom), always two elements of $\mathbf{\Omega}^{\alpha}$ are nonvanishing (Table 2). For Frenkel excitonic resonance states, these are on the diagonal, whereas for charge resonance states the off-diagonal elements are nonvanishing.

For practical calculations eq 12 has to be generalized to include nonorthogonality of the atomic orbitals (AOs). For this purpose we suggest an analysis in analogy to Mayer's bond order[22] between two atoms, μ and ν

$$\begin{aligned} B_{\mu\nu}^{\alpha} &= \sum_{\substack{a\in\mu\\ b\in\nu}} (\mathbf{D}^{\alpha\alpha,[AO]}\mathbf{S}^{[AO]})_{ab}(\mathbf{D}^{\alpha\alpha,[AO]}\mathbf{S}^{[AO]})_{ba}\\ &= \sum_{\substack{a\in\mu\\ b\in\nu}} (\mathbf{D}^{\alpha\alpha,[AO]}\mathbf{S}^{[AO]})_{ab}(\mathbf{S}^{[AO]}\mathbf{D}^{\alpha\alpha,[AO]})_{ab} \end{aligned} \quad (13)$$

where $\mathbf{D}^{\alpha\alpha,[AO]}$ is the (symmetric) one-electron density matrix of state α in the AO basis and $\mathbf{S}^{[AO]}$ is the AO overlap matrix. The summations are performed over the basis functions on atoms μ and ν. Using this form, the charge transfer number between fragments A and B can be defined by inserting the transition density matrix instead of the state density matrix:

$$\Omega_{AB}^{\alpha} = \frac{1}{2} \sum_{\substack{a\in A \\ b\in B}} (\mathbf{D}^{0\alpha,[AO]}\mathbf{S}^{[AO]})_{ab}(\mathbf{S}^{[AO]}\mathbf{D}^{0\alpha,[AO]})_{ab} \tag{14}$$

Then the sum

$$\Omega^{\alpha} = \sum_{A,B} \Omega_{AB}^{\alpha} = \frac{1}{2}\mathrm{Tr}(\mathbf{D}^{0\alpha,[AO]}\mathbf{S}^{[AO]}(\mathbf{D}^{0\alpha,[AO]})^{T}\mathbf{S}^{[AO]}) = \frac{1}{2}\mathrm{Tr}(\mathbf{D}^{0\alpha,[MO]}(\mathbf{D}^{0\alpha,[MO]})^{T}) \tag{15}$$

is invariant to any basis set transformation, demonstrating that squared density matrix elements appear to be a useful choice for our analysis (T denotes the matrix transposition, and **C** is the AO−molecular orbital (MO) transformation matrix; see section 3 for transformation rules). For a normalized configuration interaction singles (CIS) wave function, Ω^{α} is exactly 1 (cf. ref 13), and for any other excited-state wave function dominated by a one-electron transition, it should be close to 1.

In a system of two chromophores the quantity

$$\Delta^{\alpha}q_{12} = (\Omega_{12}^{\alpha} - \Omega_{21}^{\alpha})/\Omega^{\alpha} \tag{16}$$

represents the net charge shifted from fragment 1 to fragment 2 due to the excitation. Such a relation was shown to hold exactly in the case of CIS,[12,13] but it should give the correct trend also in cases where the electronic excitation can be described by a one-electron transition.

2.3. Collective Information. While a density matrix analysis as described above can be used to obtain a detailed analysis of the structures of excited states, cf. refs 8 and 13, it is in many cases also highly desirable to have even more compact descriptors. In an extension to the L_d and L_c values of ref 8, we will describe how the above information can be compressed to retrieve the most interesting physical information in a compact form. This is of particular importance for polymers or extended systems with a large number of chromophores. In the following we will drop the superscript α for simplicity, but it should be remembered that all these descriptors yield one value per electronic state at every geometry. In all formulas it is assumed that the normalization factor Ω deviates only slightly from 1. Otherwise, an analysis based only on the one-electron transition density matrix may not be suitable, and generalized expressions using two-electron transition density matrices might be necessary; cf. ref 12.

The charge transfer character (CT) is defined by summing over the off-diagonal elements, yielding

$$\mathrm{CT} = \frac{1}{\Omega} \sum_{\substack{A \\ B\neq A}} \Omega_{AB} \tag{17}$$

which corresponds to the total weight of configurations where the initial and final orbitals are situated on different fragments. CT assumes the value 1 for all completely charge separated states (Figure 1, right), whereas it is 0 for locally excited or Frenkel excitonic states (Figure 1, left).

Another interesting question refers to the extent of the delocalization of the excitation over fragments. For this purpose we will use the concept of a participation ratio to compute the number of fragments participating in the excitation; cf. refs 23 and 24. To consider the general case of a nonsymmetric **Ω** matrix, the definition is split into two parts. The participation ratio (PR) of the initial orbital or hole is defined as

$$\mathrm{PR_I} = \frac{\Omega^2}{\sum_A (\sum_B \Omega_{AB})^2} \tag{18}$$

to represent over how many fragments the hole is delocalized. The sum in parentheses considers all configurations where the initial orbital lies on a specific fragment A and goes over final orbitals on any possible fragment. Also in a similar way for the final orbital

$$\mathrm{PR_F} = \frac{\Omega^2}{\sum_B (\sum_A \Omega_{AB})^2} \tag{19}$$

The average of these two quantities

$$\mathrm{PR} = (\mathrm{PR_I} + \mathrm{PR_F})/2 \tag{20}$$

is used to represent the number of fragments involved in the excited state. Considering the above examples (section 2.1), this appears to be a suitable measure for delocalization, giving PR = 1 for all the localized states (Table 1) and PR = 2 for all the delocalized states (Table 2).

The above formalism requires the construction of two separate quantities, $\mathrm{PR_I}$ and $\mathrm{PR_F}$. This was avoided in ref 8 by considering only diagonal elements. The quantity

$$\mathrm{PR_{diag}} = \frac{(\sum_A \Omega_{AA})^2}{\sum_A (\Omega_{AA})^2} \tag{21}$$

would correspond to L_d of ref 8 (with the only exception that squared rather than absolute values of density matrix elements are taken here). However, the advantage of the present definition of PR is that it is also well-defined when the diagonal elements of **Ω** are 0 as this is the case in charge transfer and charge resonance states ($|1^-2^+\rangle$ and $|1^+2^-\rangle$ in Table 1, δ and ρ in Table 2).

The coherence length (COH) of the excited state, which is related to the average electron−hole separation, can be defined following the ideas of ref 8 as

$$\mathrm{COH} = \frac{1}{\mathrm{PR}} \frac{\Omega^2}{\sum_A \sum_B \Omega_{AB}^{\ 2}} \tag{22}$$

Whereas PR gives the total spatial distribution of the exciton as a quasiparticle, COH relates to the intrinsic structure of the exciton. The measure is largest when locally excited and charge transfer configurations are participating in equal amounts. For loosely bound excitons (all elements of **Ω** are the same value) COH = PR, whereas for pure Frenkel excitons (only diagonal elements of **Ω** are nonzero) COH = 1 (cf. ref 8).

Finally, quantities are described which are applicable mostly if a linear arrangement of the fragments is present. The average position (POS) of the initial orbital (hole) is computed as

$$\mathrm{POS_I} = \frac{\sum_A A(\sum_B \Omega_{AB})}{\Omega} \tag{23}$$

the position of the final orbital (electron) as

$$\mathrm{POS_F} = \frac{\sum_B B(\sum_A \Omega_{AB})}{\Omega} \tag{24}$$

and the mean position as

$$\mathrm{POS} = (\mathrm{POS_I} + \mathrm{POS_F})/2 \tag{25}$$

Considering the idealized dimer states (Tables 1 and 2), $|1^*2\rangle$ yields POS = 1, $|12^*\rangle$ yields POS = 2, and all charge transfer and delocalized states show POS = 1.5.

The signed net charge transfer length (CT_{net})

$$CT_{net} = POS_F - POS_I \tag{26}$$

is computed as the difference between the centers of charge of the electron and hole. Considering Table 1, $|1^-2^+\rangle$ has $CT_{net} = -1$ and $|1^+2^-\rangle$ yields $CT_{net} = 1$. All other states in Tables 1 and 2 have no net transfer of charge.

2.4. Natural Transition Orbitals. Natural transition orbitals (NTOs) can be used to create a compact representation of an electronic excited state by reducing the number of configurations required to describe the most important features of a transition.[14−16] As opposed to a state density, it is not generally possible to diagonalize a transition density since it is not symmetric. However, a singular value decomposition scheme can be used where the decomposition of the transition density matrix using unitary matrices **U** and **V** may be written as

$$\mathbf{D}^{0\alpha,[MO]} = \mathbf{U}\ \mathrm{diag}(\sqrt{\lambda_1}, \sqrt{\lambda_2}, ...)\ \mathbf{V}^T \tag{27}$$

U denotes a set of initial (hole) orbitals and **V** the final (electron) orbitals, and the λ_i are the weights of the corresponding transitions. Typically only a very small number of configurations are necessary to describe the states in this way, and plotting the orbitals gives a compact graphical representation of the excited state (as shown, for example, in refs 11, 15, 16, and 20). In general, **U** and **V** are different. However, in the case of a CIS-type wave function (where only the occupied virtual block of $\mathbf{D}^{0\alpha,[MO]}$ is nonvanishing), it is possible to choose **U** = **V** due to degenerate singular values. Then the natural transition orbitals are in fact identical to the natural orbitals of the corresponding CIS wave function.[25]

An interesting property of this decomposition, which has been pointed out in ref 20, is that for resonant delocalized states always two significant nonvanishing singular values are present. This is represented in eqs 5−8: Two excitation operators are needed for constructing the excited state. This is true independent of whether localized or delocalized orbtials are used (cf. ref 18), and there is no orbital basis that could be used to construct the excited state with only one transition. To formalize this concept, we use a participation ratio[23,24] expression for the number of singular values to define the natural transition orbital participation ratio:

$$PR_{NTO} = \frac{(\sum_i \lambda_i)^2}{\sum_i \lambda_i^2} = \frac{4\Omega^2}{\sum_i \lambda_i^2} \tag{28}$$

where the second equality holds because of the fact that λ_i are the eigenvalues of the product matrix $\mathbf{D}^{0\alpha,[MO]}(\mathbf{D}^{0\alpha,[MO]})^T$. The analogous expression was called the collectivity index in ref 13. It is a lower bound to the number of nonzero singular values (N_{SVD}),[13] where $PR_{NTO} = N_{SVD}$ only in the case that all nonzero singular values have the same magnitude. In this sense PR_{NTO} counts how many different NTOs are participating and thus how many transitions are necessary to describe the excited state. In combination with the considerations at the beginning of this paragraph, PR_{NTO} could be seen as an intrinsic measure giving information about electronic resonances that does not require the definition of any fragments. A decrease of PR_{NTO} can have two different implications. In the first case this decrease could coincide with a localization of the exciton and therefore a decrease in PR (eq 20). On the other hand, if a large value of PR coincides with a low PR_{NTO}, this means that a larger spatial delocalization is combined with a coherent homogeneous excitation which should concur with a large COH (eq 22). An example for this situation is the $|\chi^{-/+}\rangle$ state given in eq 9. Further formal discussion of these relations is given in the Supporting Information (section S5). Note that the number of nonzero singular values (and thus PR_{NTO}) was also considered as a measure of electron correlation in the excited-state wave function.[25] In the present context this can be understood by the fact that an excitonic or charge resonance state requires some additional electron correlation as compared to a homogeneous excitation (the electron and hole move in a somewhat correlated fashion as they are always on the same or on different fragments, respectively).

3. COMPUTATIONAL DETAILS

As the first example a stacked arrangement of two face-to-face formaldehyde molecules at their ground-state minimum geometries separated by 3.5 Å in a parallel arrangement was considered. The calculations of the electronic states were performed using multireference configuration interaction with single and double excitations (MR-CISD) using a complete active reference space of eight electrons in six orbitals (π, n, and π^* on each molecule). The orbitals were generated by using a complete active space self-consistent field wave function with eight electrons and six orbitals (CASSCF(8,6)) in the same active space as selected for the MR-CISD reference space given just above. Averaging over the first three states was performed, and the aug-cc-pVDZ basis set was used.[26] Energies, density matrices, and analytic nonadiabatic coupling vectors at the MR-CISD level were computed with the COLUMBUS 7.0 program package.[27−32]

The electronic states of the remaining systems (naphthalene dimer, diadenine stack, and phenylenevinylene oligomer $(PV)_6P$) were treated using the algebraic diagrammatic construction to second order (ADC(2))[33] with the resolution of the identity approximation (RI).[34−37] The geometry of the naphthalene dimer was constructed by first optimizing the monomer at the RI-MP2/SVP[38] level and then placing two monomers in a face-to-face arrangement. The calculations were performed in D_{2h} symmetry where the long and short molecular axes were arranged in the x- and y-directions, respectively, and the z-axis was perpendicular to the molecular planes. The aug-cc-pVDZ basis set[26,39] was used, considering that diffuse functions are necessary to guarantee a correct orbital overlap interaction for large intermolecular distances.[40] The geometry for the adenine dimer was constructed by first optimizing the adenine monomer at the RI-MP2/SVP[38] level and then inserting this structure by a least-squares fit[41] into an arrangement of idealized B-DNA geometry, as created with the Nucleic program distributed with Tinker.[42] Vertical excitations for the dimer were computed at the RI-ADC(2)/TZVP[43] level. RI-MP2/SV(P) ground-state geometry optimization was performed for $(PV)_6P$. For vertical excitations and the excited-state optimization the RI-ADC(2)/SV(P) method was used. The structure was restricted to C_{2h} symmetry for computational efficiency. All RI-MP2 and RI-ADC(2) calculations were performed using TURBOMOLE 6.3.[44]

Corrections for basis set superposition error (BSSE)[45] are quite important in the description of excimers,[46] considering the fact that intermolecular separations may be significantly smaller than in ground-state complexes. Unfortunately, in the

case of strongly interacting chromophores a consistent definition of a counterpoise correction[45] is quite challenging. In the case of separated Frenkel excitonic and charge transfer contributions, it is conceivable to compute a state-specific correction by considering appropriate locally excited and ionic states of the monomer. However, if different monomer states interact and excitonic and charge transfer contributions mix (cf. section 4.2), such a task does not seem feasible. Thus, in the case of the naphthalene dimer the total energies of all excited states were corrected with the counterpoise correction computed for the ground state as a compromise. The assumption behind this is that one electron promoted into a valence orbital should only have a minor contribution to the BSSE as opposed to the remaining electrons, which are largely unaffected by the excitation. The BSSE-corrected total energy of state α in the dimer $E^{\alpha}_{\mathrm{dimer,corr}}$ was computed from the uncorrected energy $E^{\alpha}_{\mathrm{dimer}}$ as

$$E^{\alpha}_{\mathrm{dimer,corr}} = E^{\alpha}_{\mathrm{dimer}} + 2(E^{0}_{\mathrm{monomer,[monomer]}} - E^{0}_{\mathrm{monomer,[dimer]}}) \tag{29}$$

where $E^{0}_{\mathrm{monomer,[monomer]}}$ and $E^{0}_{\mathrm{monomer,[dimer]}}$ are the MP2 ground-state energies of one of the equivalent monomers using the AO basis set of the monomer and dimer, respectively. It may be noted here that in this approach vertical excitation energies are uncorrected.

Fragments, as necessary for the summations in section 2.3, were assigned as follows. In the first three cases the fragments corresponded to the two separate molecules in the dimer. For $(PV)_6P$ we formally cut the C=C double bonds of the vinyl moieties to obtain the fragment definitions. This choice was made to obtain a set of analogous fragments, which also preserved the overall symmetry of the system.

For the MR-CISD calculations the exact one-electron transition density matrices as given by the COLUMBUS program system were used. Considering that for ADC(2) calculations these were not available to us, the singly excited cluster amplitudes were chosen instead to represent the excitation. This choice was made considering the close relationship between these quantities and because of the fact that it is just these amplitudes which are usually considered for manually analyzing excited states. To reduce inconsistencies, normalization against the sum of the weights, Ω (eq 15), was performed. Moreover, it was checked that this normalization factor was always close to 1. Whereas exact transition density matrices would be desirable if available, we want to point out that this approximate method opens a pathway that significantly enhances the general applicability and ease of implementation of our analysis procedure.

MO coefficients were obtained in terms of Cartesian atomic orbitals in MOLDEN format[47] as supplied by COLUMBUS and TURBOMOLE. The MO−AO transformations of density and overlap matrices were performed according to ref 48:

$$\mathbf{D}^{[\mathrm{AO}]} = \mathbf{C}\mathbf{D}^{[\mathrm{MO}]}\mathbf{C}^{\mathrm{T}} \tag{30}$$

$$\mathbf{S}^{[\mathrm{AO}]} = \mathbf{C}^{-1,\mathrm{T}}\mathbf{S}^{[\mathrm{MO}]}\mathbf{C}^{-1} = \mathbf{C}^{-1,\mathrm{T}}\mathbf{C}^{-1} \tag{31}$$

This led to the following expressions for the matrix products of eq 14:

$$\mathbf{D}^{[\mathrm{AO}]}\mathbf{S}^{[\mathrm{AO}]} = \mathbf{C}\mathbf{D}^{[\mathrm{MO}]}\mathbf{C}^{\mathrm{T}}\mathbf{C}^{-1,\mathrm{T}}\mathbf{C}^{-1} = \mathbf{C}\mathbf{D}^{[\mathrm{MO}]}\mathbf{C}^{-1} \tag{32}$$

$$\mathbf{S}^{[\mathrm{AO}]}\mathbf{D}^{[\mathrm{AO}]} = \mathbf{C}^{-1,\mathrm{T}}\mathbf{D}^{[\mathrm{MO}]}\mathbf{C}^{\mathrm{T}} \tag{33}$$

where $\mathbf{C}$ is the MO coefficient matrix and the overlap in the MO basis $\mathbf{S}^{[\mathrm{MO}]}$ is a unit matrix.

Some of the mathematical formulas were derived or verified by using the Mathematica 5.2[49] program. An efficient implementation of the matrix operations was achieved by using the NumPy tools.[50] Plotting of the computed natural transition orbitals was performed with the Jmol program package.[51] The code described here is freely available and is currently distributed as a test version,[52] providing interfaces to the COLUMBUS and TURBOMOLE programs for applications with the CASSCF, MR-CI, ADC(2), CC2, and time-dependent density functional theory (TDDFT) methods.

4. RESULTS AND DISCUSSION

4.1. Formaldehyde Dimer. In this section the interaction between the lowest excited states of two stacked formaldehyde molecules, which are of nπ^* character, is considered. An asymmetry, leading to nonequivalence of the two monomers and a corresponding localization of the excitation, is introduced by altering the asymmetric stretch coordinate

$$\Delta R = 2^{-1/2}(R_{\mathrm{CO},1} - R_{\mathrm{CO},2}) \tag{34}$$

in the two CO distances. A more detailed explanation of the underlying physical models in such a case is given in ref 40. Here only the most important results are presented. In Figure 2 potential curves along ΔR, the POS value, and the nonadiabatic

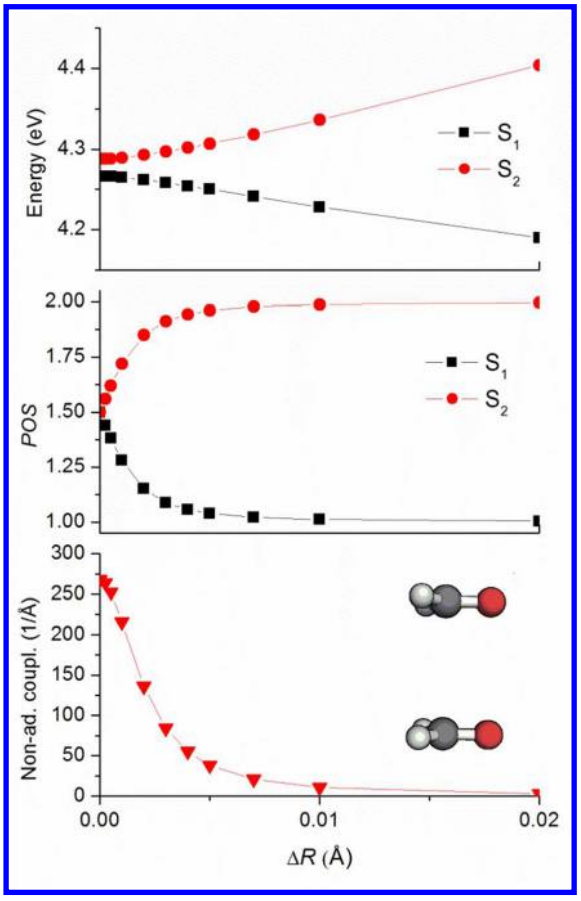

Figure 2. MR-CISD state energies, position (POS) values, and nonadiabatic couplings projected onto ΔR for two interacting nπ^* states of two stacked formaldehyde molecules separated by a distance of 3.5 Å.

coupling projected onto ΔR, i.e., $\langle\varphi_1|\partial/(\partial(\Delta R))\varphi_2\rangle$ (where φ_1 and φ_2 are the wave functions of the two electronic states), are presented for the S_1 and S_2 states of the formaldehyde dimer. At the symmetric geometry there is a small gap of 0.0216 eV between S_1 and S_2, which derives from the excitonic coupling. At this point, the S_1 and S_2 wave functions are evenly delocalized ($POS_1 = POS_2 = 1.5$, PR = 2.0). A large component of the nonadiabatic coupling vector between these two states along the ΔR direction (268 $Å^{-1}$) indicates that the wave functions should change rapidly upon displacement. Accordingly, if the symmetry is lifted by bond length alternation, the two excited states quickly localize and already at ΔR = 0.005 Å the states are almost completely localized on either molecule (POS_1 = 1.04). Also the nonadiabatic coupling is reduced substantially.

In Table 3 a collection of complementary descriptors is presented for three different ΔR values. The small CT value found over the whole range of ΔR values considered indicates that the states are of Frenkel excitonic nature, without significant charge transfer interactions. Next the excitonic PR is shown. PR = 2.00 at ΔR = 0 reflects that due to symmetry the excited states are completely delocalized over the two fragments. At ΔR = 0.005 Å the wave function is already almost completely localized (PR = 1.08). PR_{NTO}, giving the number of configurations minimally necessary to describe a state, is about 2 for the delocalized states and goes to 1 as the excited states are localized. This is just what corresponds to the idealized model.[18,20] The fact that PR is somewhat lower than 2 at ΔR = 0 is probably due to orbital interactions, which is reflected by the fact that the CT value is not completely vanishing.

Table 3. CT, Excitonic PR, and PR_{NTO} for the S_1 State of Two Stacked Formaldehyde Molecules Separated by a Distance of 3.5 Å at Different Values of the Bond Length Alternation ΔR

ΔR (Å)	CT	PR	PR_{NTO}
0	0.005	2.00	1.95
0.002	0.005	1.35	1.33
0.005	0.004	1.08	1.08

4.2. Naphthalene Dimer. The naphthalene dimer is an interesting benchmark system where the interactions between excitonic and charge resonance states and the formation of a strongly stabilized excimer has been reported.[18,19] In the present investigation, the eclipsed dimer was chosen and the dependence of excited states on the intermolecular distance was considered. Excited states were computed at the RI-ADC(2)/aug-cc-pVDZ level. Because of the symmetry, all states are evenly delocalized in this system (PR = 2, POS = 1.5), and the amount of charge separation, CT, remains the main feature of interest. It should be noted here that also all orbitals and densities are delocalized, and therefore, an identification of charge-separated configurations is not trivial. The problem was solved by East and Lim[18] through an analysis involving a careful inspection of the symmetry properties of all the orbitals

Table 4. Excitation Energies (ΔE, eV), Oscillator Strengths (f), Charge Transfer Values, Natural Transition Orbital Participation Ratios, and Type Assignments of the Nine Lowest Energy $\pi\pi^*$ States of the Stacked Naphthalene Dimer at an Intermolecular Separation of 5.0 Å

state	ΔE	f	dominant contributions[a]	CT	PR_{NTO}	type[b]
1^1B_{2g} (S_1)	4.386	0	$11b_{1u}-11b_{3u}$ (0.49) $7a_u-11b_{2u}$ (0.45) $7b_{1g}-11b_{3g}$ (0.44)	0.00	3.93	$^1\sigma^{01+}$
1^1B_{3u} (S_2)	4.394	0.00002	$11a_g-11b_{3u}$ (−0.47) $7a_u-11b_{3g}$ (0.47) $7b_{1g}-11b_{2u}$ (0.43)	0.00	4.00	$^1\gamma^{01+}$
1^1B_{3g} (S_3)	4.709	0	$7a_u-11b_{3u}$ (0.72) $7b_{1g}-10b_{2g}$ (0.46) $7b_{1g}-11b_{2g}$ (0.38)	0.01	2.00	$^1\sigma^{00}$
1^1B_{2u} (S_4)	4.759	0.144	$7b_{1g}-11b_{3u}$ (0.67) $7a_u-10b_{2g}$ (0.50) $7a_u-11b_{2g}$ (0.42)	0.00	2.14	$^1\gamma^{00}$
3^1B_{2g} (S_{12})	5.789	0	$7a_u-11b_{2u}$ (0.53) $11b_{1u}-11b_{3u}$ (−0.53) $7b_{1g}-11b_{3g}$ (0.35)	0.04	3.54	$^1\sigma^{01-}$
3^1B_{2u} (S_{13})	5.867	0.0003	$7b_{1g}-11b_{3u}$ (−0.61) $7a_u-10b_{2g}$ (0.55) $7a_u-11b_{2g}$ (0.41)	0.94	2.00	$^1\delta^{00}$
3^1B_{3g} (S_{14})	5.874	0	$7b_{1g}-10b_{2g}$ (0.59) $7a_u-11b_{3u}$ (−0.57) $7b_{1g}-11b_{2g}$ (0.46)	0.95	1.95	$^1\rho^{00}$
3^1B_{3u} (S_{17})	6.113	2.700	$7b_{1g}-11b_{2u}$ (0.53) $11a_g-11b_{3u}$ (0.48) $7a_u-11b_{3g}$ (0.38)	0.08	3.85	$^1\gamma^{01-}$
4^1B_{3g} (S_{20})	6.283	0	$11b_{1u}-11b_{2u}$ (0.69) $11a_g-11b_{3g}$ (−0.53) $11b_{1u}-12b_{2u}$ (−0.30)	0.03	1.95	$^1\sigma^{11}$

[a]Dominant contributions to the excitation, coefficient in parentheses. [b]Nomenclature according to Figure 1 and ref 18.

involved. It will be shown how the same results can be obtained by simply considering the CT value defined above. Moreover, the CT value provides a well-defined quantifier for measuring the gradual mixing between excitonic and charge resonance contributions, which will be illustrated for the case of excimer formation.

In Table 4 a summary of the lowest energy singlet $\pi\pi^*$ excited states at an intermolecular distance of 5.0 Å is presented. The Rydberg states, which are also present at this energy range, are not shown. First, it can be seen that the states are clearly separated into Frenkel-type excitonic resonance states (CT ≈ 0) and charge resonance states (CT ≈ 1). Mixing between these types of states occurs only at smaller intermolecular separations (cf. refs 18 and 19), a process which will be described later. The first two excited states (1^1B_{2g}, 1^1B_{3u}) are of Frenkel type (CT = 0.0). An analysis of the orbitals and transition moments shows that these states derive from the lowest singlet excited state (S^{01+}, ^1L_b) of naphthalene, forming the $^1\sigma^{01+}$ and $^1\gamma^{01+}$ states in the nomenclature of ref 18 (cf. Figure 1). The 1^1B_{2g} state has zero oscillator strength for symmetry reasons, and for 1^1B_{3u} this value is also almost vanishing. This is in agreement with the small exciton splitting of only 0.0087 eV between these two states. PR_{NTO} is about 4 for these two states: two configurations are already needed to describe the corresponding monomer states,[18] and this value is doubled in the resonant delocalized state. The next two excited states (1^1B_{3g}, 1^1B_{2u}) are again of Frenkel type (CT = 0.0). Both states derive from the S_2 (S^{00}, ^1L_a) state of naphthalene and may be designated as the $^1\sigma^{00}/^1\gamma^{00}$ excitonic pair. The oscillator strength of the γ state is 0.144, and an excitonic splitting of 0.049 eV is present. Considering the remaining states, it may be observed that the 3^1B_{2u} and 3^1B_{3g} states are composed of the same orbital contributions as 1^1B_{3g} and 1^1B_{2u} but that they show CT ≈ 1. They are the charge resonance states related to S^{00} (designated $^1\delta^{00}$ and $^1\rho^{00}$). Thus, in summary, a complete set of four excited states deriving from the S^{00} monomer transition could be identified (cf. Figure 1, bottom). PR_{NTO} reveals that for all four of the resonant states in the S^{00} series two configurations are significantly involved, which is consistent with the idealized case[18,20] shown in eqs 5−8. Here it may be noticed that the singular value decomposition reduced the number of configurations needed to describe the excited state: Whereas $7b_{1g}-10b_{2g}$ and $7b_{1g}-11b_{2g}$ amount to two different configurations in Hartree−Fock orbitals, these are reduced to one configuration where the virtual NTO is a linear combination of the $10b_{2g}$ and $11b_{2g}$ orbitals. The 3^1B_{2g} and 3^1B_{3u} states form another pair of excitonic resonance states ($^1\sigma^{01-}/^1\gamma^{01-}$). In agreement with the larger oscillator strength of the γ state (2.700), the excitonic splitting is also larger (0.324 eV). The final state shown (4^1B_{3g}) is again of Frenkel excitonic type and may be designated $^1\sigma^{11}$. In the energetic region considered here only two states (3^1B_{2u}, 3^1B_{3g}) with non-vanishing CT contribution, belonging to the S^{00} monomer state, were found. The charge resonance combinations of the S^{01+}, S^{01-}, and S^{11} monomer states lie at higher energies and are not presented in Table 4. For a discussion of these states, the reader is referred to ref 18.

Next the geometry dependence of the excited states with respect to the intermolecular distance of the naphthalene molecules is examined, and in particular it will be outlined how the four states deriving from the S^{00} monomer state interact to form the strongly stabilized excimer. For this purpose the excited-state energies and CT and PR_{NTO} properties of these states are presented in Figure 3. Potential curves of the 1^1B_{2g} and 1^1B_{3u} states are presented for comparison. At 5.0 Å and

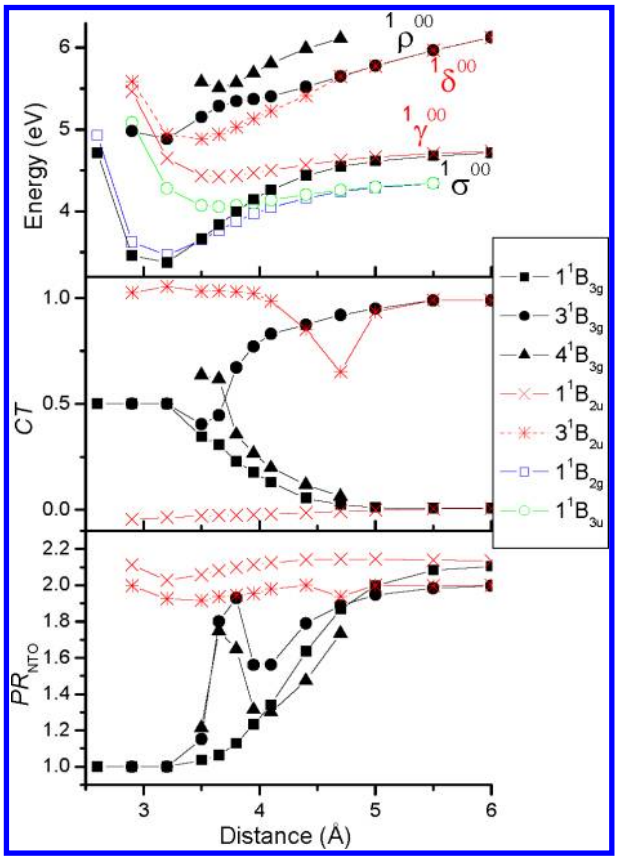

Figure 3. Counterpoise-corrected state energies relative to the ground state at infinite separation, CT, and PR_{NTO} for the lowest singlet $\pi\pi^*$ states of B_{3g} (black) and B_{2u} (red) symmetry of a face-to-face stacked naphthalene dimer at different intermolecular distances. The energies of the lowest singlet excited states of B_{2g} (blue) and B_{3u} (green) symmetry are presented as well. The state labels correspond to the assignments at 5.0 Å; whenever crossings between Rydberg and $\pi\pi^*$ states occurred, the indices were adjusted accordingly.

longer intermonomer separations, a clear distinction between Frenkel excitonic and charge-separated states, as described above, can be seen. 1^1B_{3g} and 1^1B_{2u} form the almost degenerate excitonic $^1\sigma^{00}/^1\gamma^{00}$ pair with CT ≈ 0, whereas for the corresponding charge resonance states 3^1B_{3g} ($^1\rho^{00}$) and 3^1B_{2u} ($^1\delta^{00}$) CT ≈ 1. At this large separation all these states show PR_{NTO} ≈ 2 (with deviations of less than 0.2). When the intermolecular distance is decreased, a splitting between 1^1B_{3g} and 1^1B_{2u} as well as 3^1B_{3g} and 3^1B_{2u} is observed due to excitonic and charge resonance interactions, respectively. At the same time also the excitonic splitting between the 1^1B_{2g} and 1^1B_{3u} states is raised. As the distance is decreased further, the B_{2u} states (Figure 3, red) retain their diabatic character, i.e., $CT(1^1B_{2u})$ ≈ 1 and $CT(3^1B_{2u})$ ≈ 0, and their PR_{NTO} stays at about 2, also indicating that no changes occur. There is only a small spike in CT at 4.7 Å, which seems to be caused by an interaction with a Rydberg state. It may be noted that at very small intermolecular separations the CT value of 3^1B_{2u} goes slightly below 0, whereas that of 1^1B_{2u} goes above 1. This result is present because of slightly negative Ω^{α}_{AB} values, which according to eq 14 may be obtained if the overlap is strong. It is related to the existence of negative Mulliken populations.[53] In

Table 5. Excitation Energies (ΔE, eV), Oscillator Strengths (f), Dipole Moments (μ, D), Statistical Descriptors, and Type Assignments for the First 10 Excited States of a Diadenine Stack in B-DNA Geometry

state	ΔE	f	μ	POS	PR	CT	CT_{net}	PR_{NTO}	type
S_1	5.013	0.009	2.84	1.56	1.97	0.02	0.01	1.98	nπ^*
S_2	5.022	0.001	2.99	1.45	1.98	0.02	0.01	1.99	nπ^*
S_3	5.104	0.046	4.57	1.80	1.48	0.04	−0.02	1.54	$\pi\pi^*$
S_4	5.193	0.054	4.46	1.36	1.84	0.03	0.00	2.75	$\pi\pi^*$
S_5	5.225	0.007	5.62	1.43	1.96	0.03	0.00	3.26	$\pi\pi^*$
S_6	5.307	0.345	4.95	1.39	1.90	0.03	0.00	2.07	$\pi\pi^*$
S_7	5.724	0.005	3.64	1.11	1.25	0.02	0.01	1.23	nπ^*
S_8	5.743	0.001	2.87	1.89	1.25	0.01	−0.01	1.24	nπ^*
S_9	5.854	0.015	12.20	1.49	1.09	0.92	−0.92	1.07	$\pi\pi^*$ (CT)
S_{10}	6.128	0.000	4.39	1.85	1.34	0.03	−0.01	1.47	nπ^*

spite of being an artifact in the present context, it should not affect any of the qualitative implications of the results. The situation is more complicated for the B_{3g} states (Figure 3, black). 1^1B_{3g} does not remain a pure Frenkel exciton but gains part of the charge transfer character of 3^1B_{3g}, which means that these states are no longer well-defined as $^1\sigma^{00}$ and $^1\rho^{00}$ states. Additionally, at 3.8 Å there is an avoided crossing between 3^1B_{3g} and 4^1B_{3g}. 4^1B_{3g} now becomes the continuation of the $^1\rho^{00}$ state, which can be seen by the fact that the CT values of these two states cross. Interestingly, PR_{NTO} shows a spike at the avoided crossing for the two states involved because of the fact that two configurations mix at this point. At about 3.5 Å intermolecular separation the 1^1B_{3g} and 1^1B_{2g} states cross, making 1^1B_{3g} the lowest singlet excited state overall (cf. ref 18.). The excimer minimum lies at 3.2 Å intermolecular separation. It forms a deep potential well on the 1^1B_{3g} potential surface, stabilized by 1.38 eV with respect to infinite separation. This value should be seen as an estimate, considering that a precise calculation of the interaction energy is highly challenging. Already at the ground-state minimum, the MP2 method overestimates the interaction energy by about 0.1−0.2 eV compared to the much more computationally intensive CCSD(T) reference,[54] and the discrepancies may be somewhat enhanced at smaller separations and for excited states. Moreover, basis set superposition effects play a significant role at such small intermolecular separations.[46] The counterpoise correction term for the ground state, $2(E^0_{monomer,[monomer]} - E^0_{monomer,[dimer]}) = 0.435$ eV (eq 29), was added, but this is just an approximation for the excimer state. However, in spite of a possible error of a few tenths of an electronvolt, it can be assumed that the description of the physical processes and the changes occurring in the electronic structure are qualitatively correct.

When the excimer minimum is approached, the CT values of the two B_{3g} states converge to 0.5; i.e., there is an equal probability for the electron and hole to be on the same or different molecules. The 1^1B_{3g} state is now described by only one configuration (corresponding to the $7a_u-11b_{3u}$ transition in Table 4), which means that PR_{NTO} is reduced to 1. According to eq 9, this situation may also be understood in the sense that the excimer state is an equal mixture of all four states in the upper part of Figure 1 (1^*2, 12^*, 1^+2^-, 1^-2^+). Thus, in accordance with refs 18 and 55, excitonic and CT interactions are both active in the stabilization of the excimer. In the language of ref 8 this situation also means that the coherence size now spans both molecules (COH = 2 according to eq 22). In this sense, the excimer can be explained neither by excitonic coupling nor by charge transfer, but only a coherent interaction, leading to a homogeneous excited state, can induce this strong stabilization.

4.3. Nucleobase Stacks. The nature of excited states in nucleobases has been intensively discussed using a large variety of experimental and computational methods. A question of particular importance was over how many bases the excited states are distributed and whether base−base interactions are of excitonic or charge transfer type.[3−7] In this section the analysis of a diadenine stack in idealized B-DNA geometry is performed. The two bases have the same geometry but are not exactly equivalent because of the twisted arrangement. Therefore, the electronic states are not completely delocalized; cf. ref 56. In Table 5 the excitation energies, oscillator strengths, and statistical descriptors of the first 10 excited states of the stacked dimer are shown. Additionally, the type of excitation (nπ^* or $\pi\pi^*$), obtained from visual analysis of the orbitals, is presented. The eight lowest energy states can be identified with excitonic combinations of the four lowest states of the isolated adenine.[57] S_1 and S_2 form a pair of corresponding nπ^* states, separated by a gap of 0.0091 eV. Considering the fact that the states are almost completely delocalized (POS ≈ 1.5), the excitonic coupling between these two states can be obtained as 0.0045 eV, which is similar to the value of 0.006 eV of ref 56. For these states $PR_{NTO} \approx 2.0$, which corresponds to idealized simple excitonic states. The following four states, S_3-S_6, are of $\pi\pi^*$ nature and derive from the L_a and L_b states of adenine. S_7 and S_8 form another pair of nπ^* states. These states are somewhat more localized, so that the splitting of 0.019 eV is in part due to asymmetry and in part due to the excitonic coupling. S_9 is an almost complete charge transfer state (CT = 0.92). Compared to the naphthalene dimer example, there are no charge resonance interactions here, but the charge transfer is directed ($CT_{net} = -0.92 = -CT$). This is also reflected by the large dipole moment, $\mu = 12.2$ D. Finally, a partially delocalized nπ^* state (S_{10}) can be seen. In summary, it could be shown how a large amount of quantitative physical information could be extracted from this system. A more extended study using these procedures to analyze realistic DNA fragments has been accepted for publication.[58]

4.4. Poly(phenylenevinylene)-Conjugated Organic Polymers. Recently, conjugated organic polymers have attracted a lot of interest for applications in photovoltaic devices,[10,59] and it is of particular interest to gain clear insight into the excited states involved. These are in many cases quite complex, considering that usually many molecular orbitals are involved and that different exciton bands may overlap. An analysis in terms of transition density matrices[8] is therefore convenient by reducing the representation to a form

independent of the number of orbitals involved. Additionally, as shown below, it may also give insight into excitonic structure, which would be hidden by simply considering orbitals. We performed RI-ADC(2) calculations on a phenylenevinylene oligomer, $(PV)_6P$ (see Figure 4) at its S_0 and S_1 minimum geometries, as reported in detail in ref 60.

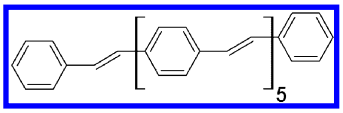

Figure 4. Structural formula of the phenylenevinylene oligomer $(PV)_6P$.

In Table 6 information about the excited states of $(PV)_6P$ at the ground-state minimum is presented. S_1 (1^1B_u) is the bright state, carrying almost all the oscillator strength. The number of fragments participating in this excited state (PR) is 5.53. This state shows a significant coherence length (COH = 3.90), which means that this state has a large electron−hole separation and cannot be viewed as a Frenkel exciton over PV units. This state is dominated by one major transition ($14b_g-14a_u$), and accordingly, PR_{NTO} is low at 1.59. In the last row of Table 6, the plot of the **Ω** matrix with respect to the seven fragments is shown. The diagonal length represents the spatial extent of the excitons, whereas the off-diagonal elements, corresponding to charge transfer configurations, mark coherences between the fragments.[8] The S_1 state shows a diagonal length over a large part of the system. The off-diagonal components indicate that there is a significant amount of electron−hole separation at least between neighboring PV units. S_2 (2^1A_g) and S_3 (2^1B_u) show a structure very similar to that of S_1, except that one and two nodal planes are present. These can therefore be interpreted as higher states of the same exciton band. Interestingly, S_4 (3^1A_g) shows a completely different structure with a significantly more pronounced charge separation and no nodal plane. Moreover, its coherence length is significantly larger (COH = 4.98). Apparently it is the first state of a different exciton band. S_5 (4^1A_g) could be seen as the next state in the initial exciton band. S_6 (3^1B_u) has a somewhat different character with a significantly lowered coherence length (COH = 2.20) and is therefore more closely related to an ideal Frenkel exciton; cf. ref 8. Note that the presence of three distinct exciton bands corresponds nicely to results obtained using solid-state physics methodology.[61]

To rationalize the results presented above, the orbitals involved in the excited states will be considered. In this context it is of particular interest how the difference between the 2^1A_g and 3^1A_g states can be understood. The dominant contributions to the excitations are given in Table 6. The corresponding orbitals are shown in Figure 5. What can be seen is that the 2^1A_g and 3^1A_g excited states consist of the same configurations with almost identical weights. Only the signs of the components differ. As shown in eqs 5−8 and ref 18, such differences can have a significant influence on the properties of the excited state. It is however quite difficult to deduce any of these properties in a canonical orbital representation.

To get a different perspective of these states, the natural transition orbitals (eq 27) are plotted in Figures 6 and 7. In this representation a clear difference is visible. The 2^1A_g state (Figure 6) can be represented by two transitions involving orbitals that are fairly evenly localized over the whole system except for the central phenyl moiety. This is in agreement with the structure and nodal plane of **Ω** as shown in Table 6. It can be seen that the two main initial and final orbitals are each of very similar shape, with the only difference being the symmetry with respect to a rotation around the center of the molecule. It may thus be understood that the excitation could also be represented by two rather localized excitations on either half of the molecule. More information about this fact and orbital plots are given in the Supporting Information (section S6). The natural transition orbitals of 3^1A_g (Figure 7) have a significantly different structure. In the first transition, shown at the top, the initial orbital is clearly localized in the center of the molecule, whereas the final orbital is distributed over the sides. The second contribution shows the opposite feature. In both cases it is seen that there is a significant participation of the central phenylene, which corresponds to the fact that there is no clear

Table 6. Excitation Energies (Δ*E*, eV), Oscillator Strengths (*f*), Statistical Descriptors, Dominant Contributions to the Excitation, and Plots of Ω for the Lowest Singlet Excited States of $(PV)_6P$ at the Ground-State Minimum Geometry

	S_1 (1^1B_u)	S_2 (2^1A_g)	S_3 (2^1B_u)	S_4 (3^1A_g)	S_5 (4^1A_g)	S_6 (3^1B_u)
ΔE	3.154	3.557	3.995	4.225	4.392	4.468
f	5.66	0	0.61	0	0	0.02
PR	5.53	6.32	6.69	5.14	6.30	3.80
COH	3.90	3.38	3.03	4.98	3.04	2.20
PR_{NTO}	1.59	2.14	2.99	2.39	4.00	4.16
Dom. contr.[a]	$14b_g$-$14a_u$ (0.86)	$13a_u$-$14a_u$ (0.65)	$13b_g$-$14a_u$ (0.55)	$13a_u$-$14a_u$ (0.53)	$13a_u$-$15a_u$ (0.41)	$8b_g$-$14a_u$ (0.47)
	$13a_u$-$15b_g$ (-0.40)	$14b_g$-$15b_g$ (-0.63)	$13a_u$-$15b_g$ (0.54)	$14b_g$-$15b_g$ (0.55)	$13b_g$-$15b_g$ (0.40)	$14b_g$-$19a_u$ (0.29)
	$13b_g$-$15a_u$ (-0.22)	$13b_g$-$15b_g$ (0.22)	$14b_g$-$15a_u$ (-0.50)	$13b_g$-$15b_g$ (0.35)	$14b_g$-$16b_g$ (0.36)	$14b_g$-$20a_u$ (-0.26)
Ω						

[a]Dominant contributions to the excitation, coefficient in parentheses.

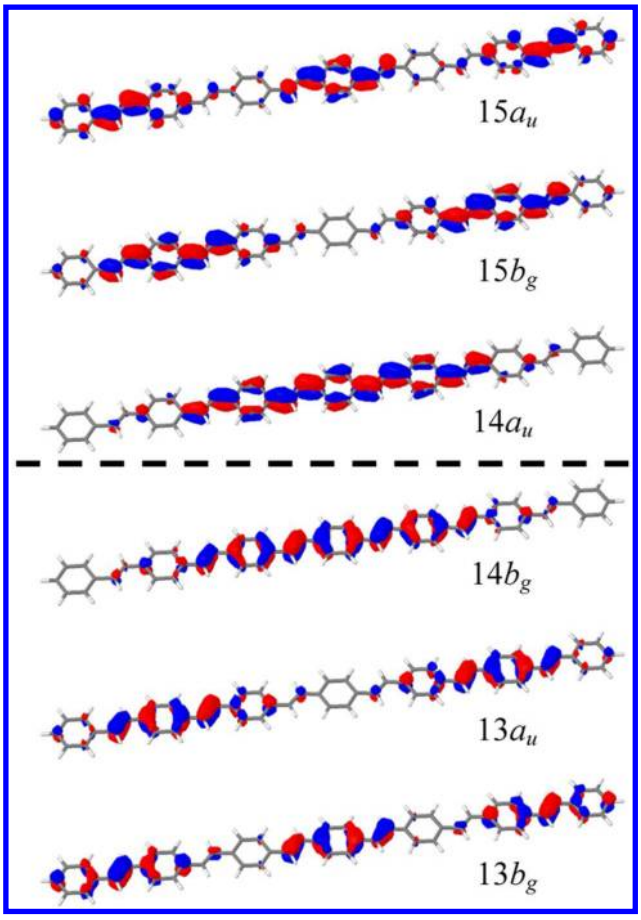

Figure 5. Frontier Hartree–Fock orbitals of $(PV)_6P$ at the optimized ground-state geometry.

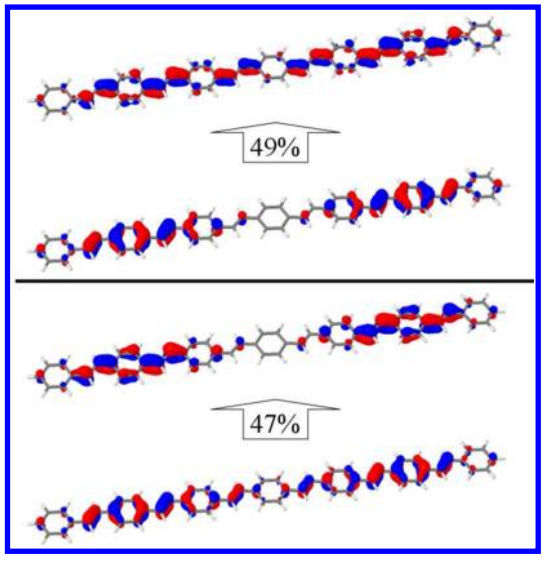

Figure 6. Two dominant pairs of natural transition orbitals for the 2^1A_g state of $(PV)_6P$.

nodal structure of **Ω** in Table 6. The fact that the initial and final orbitals are always localized on different fragments corresponds to the off-diagonal size in **Ω** and to the larger COH value.

To examine a possible localization of the excitation, a geometry optimization in the 1^1B_u state was performed (Table 7). Compared to the ground-state minimum, the 1^1B_u state is

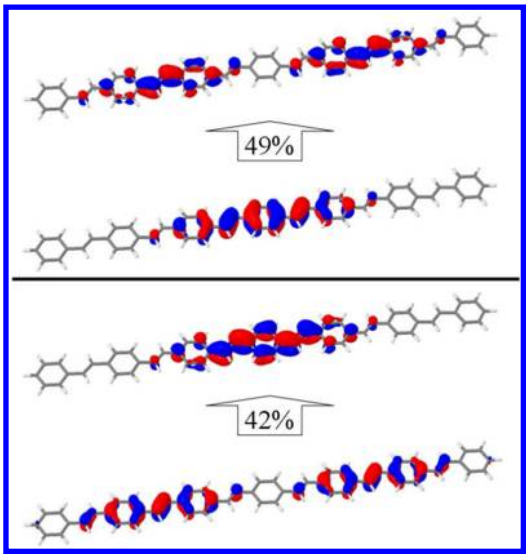

Figure 7. Two dominant pairs of natural transition orbitals for the 3^1A_g state of $(PV)_6P$.

Table 7. Excitation Energies (ΔE, eV), Oscillator Strengths (f), Statistical Descriptors, and Plots of Ω for the Lowest Excited States of $(PV)_6P$ at the S_1 (1^1B_u) Minimum Geometry

	S_1 (1^1B_u)	S_2 (2^1A_g)	S_3 (3^1A_g)	S_4 (2^1B_u)	S_5 (3^1B_u)	S_6 (4^1A_g)
ΔE	2.665	3.281	3.621	3.771	4.021	4.217
f	5.37	0	0	0.98	0.01	0
PR	5.01	6.26	4.68	6.67	5.74	6.70
COH	4.21	3.69	4.48	3.28	4.20	3.22
PR_{NTO}	1.29	2.06	2.15	2.93	2.68	4.01
Ω						

somewhat contracted upon relaxation (PR is lowered to 5.01) but remains delocalized over several fragments. This is consistent with ref 11, where the analysis was performed in terms of nuclear geometry. The coherence length is somewhat increased (COH = 4.21) and PR_{NTO} lowered, reflecting the formation of a more homogeneous coherent excited state. Interestingly, the 3^1A_g state is strongly stabilized and moves below the 2^1B_u state. The 3^1B_u state here appears to be of the same character as 3^1A_g except that it has a nodal plane.

5. CONCLUSIONS

We presented a scheme for the analysis of one-electron singlet excited states in dimers, oligomers, and extended molecular systems. Through an analysis of the one-electron transition density matrix, significant new insight can be gained over a manual wave function analysis. Quantities of immediate physical interest, such as charge separation, exciton delocalization, and coherence, can be obtained through partial summation schemes. The method is readily automatized, providing a route for statistical analysis. The general formulation of the equations allows an application to a wide variety of wave function models. So far, implementations are available for the CASSCF, MR-CI, CC2, ADC(2), and TDDFT methods. Fundamental limitations are related only to the physical properties of the excited state (i.e., only one-electron

dx.doi.org/10.1021/ct300307c | J. Chem. Theory Comput. 2012, 8, 2777–2789

excited states can be analyzed). To show the applicability of this method, we presented results on several classes of systems using different correlated ab initio wave function models.

First, for methodological purposes, excitonic interactions between the nπ^* states of two face-to-face stacked formaldehyde molecules were considered. It was shown how a displacement from the symmetric geometry led to a localization of the wave function. This process was analyzed using the above-mentioned techniques. In addition, it was pointed out how the change in the wave function properties could be related to the ab initio nonadiabatic coupling vectors.

The example of a π-stacked naphthalene dimer was used to examine the performance of our analysis scheme for states which were completely delocalized due to symmetry. In this case a differentiation between Frenkel excitonic and charge resonance states is particularly challenging because of the fact that all orbitals are evenly distributed over both fragments. The automatized analysis gave results consistent with the formal considerations of ref 18. Moreover, by systematically following the change in the wave function, when the intermolecular separation was lowered, interesting new insight into the process of excimer formation could be obtained. A mixing between excitonic and charge resonance character (cf. refs 18 and 55), yielding a homogeneous and coherent excited state, was identified as a possible cause of the strong stabilization of the excimer.

Using two stacked adenine molecules, it was shown how the analysis scheme can also be readily applied to systems with a number of interacting excited states of different character. A collection of different physical descriptors could be provided for a compact representation of the states. It was found that the lowest eight singlet excited states were excitonic combinations of the four lowest monomer states, with only a few percent of charge resonance character. The next state, S_9, was identified as a pure charge transfer state.

A phenylenevinylene oligomer was considered to test the performance of our analysis with respect to conjugated π-systems. An analysis of the vertical excitations revealed details of the excitonic structure, which remained hidden by a simple consideration of the canonical orbitals. Excited states, belonging to three different distinct exciton bands,[61] could be identified. The difference could be represented by the $\mathbf{\Omega}$ matrix and was also shown graphically in the natural transition orbital[14−16] representation. An analysis of the excited states at the S_1 minimum was presented as well.

This work was intended as a methodological outline of the working equations and as a tentative collection of potential applications of this method. More detailed investigations on the systems described are in progress.

■ ASSOCIATED CONTENT

Supporting Information

Cartesian coordinates of the molecular structures considered (Tables S1−S4), mathematical discussion of the relations among PR, COH, and PR_{NTO} (section S5), and localization of the PPV NTOs (section S6). This material is available free of charge via the Internet at http://pubs.acs.org.

■ AUTHOR INFORMATION

Corresponding Author

*E-mail: felix.plasser@univie.ac.at; hans.lischka@ttu.edu.

Notes

The authors declare no competing financial interest.

■ ACKNOWLEDGMENTS

We thank I. Burghardt for discussions and for pointing out ref 61. F.P. is a recipient of a DOC fellowship of the Austrian Academy of Sciences. This work was supported by the Austrian Science Fund within the framework of the Special Research Program and F41 Vienna Computational Materials Laboratory (ViCoM). Support was also provided by the Robert A. Welch Foundation under Grant D-0005. We also acknowledge technical support from and computer time at the Vienna Scientific Cluster (Projects 70019 and 70151).

■ REFERENCES

(1) Middleton, C. T.; de La Harpe, K.; Su, C.; Law, Y. K.; Crespo-Hernandez, C. E.; Kohler, B. *Annu. Rev. Phys. Chem.* **2009**, *60*, 217−239.
(2) Markovitsi, D.; Gustavsson, T.; Banyasz, A. *Mutat. Res., Rev. Mutat. Res.* **2010**, *704*, 21−28.
(3) Crespo-Hernandez, C.; Cohen, B.; Kohler, B. *Nature* **2005**, *436*, 1141−1144.
(4) Markovitsi, D.; Talbot, F.; Gustavsson, T.; Onidas, D.; Lazzarotto, E.; Marguet, S. *Nature* **2006**, *441*, E7−E7.
(5) Buchvarov, I.; Wang, Q.; Raytchev, M.; Trifonov, A.; Fiebig, T. *Proc. Natl. Acad. Sci. U.S.A.* **2007**, *104*, 4794−4797.
(6) Takaya, T.; Su, C.; de La Harpe, K.; Crespo-Hernandez, C.; Kohler, B. *Proc. Natl. Acad. Sci. U.S.A.* **2008**, *105*, 10285−10290.
(7) Markovitsi, D.; Vaya, I.; Gustavsson, T.; Miannay, F. A.; Douki, T. *J. Am. Chem. Soc.* **2010**, *132*, 11834−11835.
(8) Tretiak, S.; Mukamel, S. *Chem. Rev.* **2002**, *102*, 3171−3212.
(9) Wu, C.; Malinin, S. V.; Tretiak, S.; Chernyak, V. Y. *J. Chem. Phys.* **2008**, *129*, 174112.
(10) Brédas, J.-L.; Norton, J. E.; Cornil, J.; Coropceanu, V. *Acc. Chem. Res.* **2009**, *42*, 1691−1699.
(11) Nayyar, I.; Batista, E.; Tretiak, S.; Saxena, A.; Smith, D.; Martin, R. *J. Phys. Chem. Lett.* **2011**, *2*, 566−571.
(12) Prezhdo, O. V.; Luzanov, A. V. *Int. J. Quantum Chem.* **2005**, *102*, 582−601.
(13) Luzanov, A. V.; Zhikol, O. A. *Int. J. Quantum Chem.* **2010**, *110*, 902−924.
(14) Luzanov, A. V.; Sukhorukov, A. A.; Umanskii, V. E. *Theor. Exp. Chem.* **1976**, *10*, 354−361.
(15) Martin, R. L. *J. Chem. Phys.* **2003**, *118*, 4775−4777.
(16) Mayer, I. *Chem. Phys. Lett.* **2007**, *437*, 284−286.
(17) Head-Gordon, M.; Grana, A. M.; Maurice, D.; White, C. A. *J. Phys. Chem.* **1995**, *99*, 14261−14270.
(18) Lim, E. C.; East, A. L. L. *J. Chem. Phys.* **2000**, *113*, 8981−8994.
(19) Scholes, G. D.; Ghiggino, K. P. *J. Phys. Chem.* **1994**, *98*, 4580−4590.
(20) Mayer, I. *Chem. Phys. Lett.* **2007**, *443*, 420−425.
(21) Shepard, R. In *Ab Initio Methods in Quantum Chemistry II*; Lawley, K. P., Ed.; Wiley: New York, 1987; pp 63−200.
(22) Mayer, I. *Chem. Phys. Lett.* **1983**, *97*, 270−274.
(23) Pipek, J.; Mezey, P. G. *Int. J. Quantum Chem.* **1988**, *34*, 1−13.
(24) Czader, A.; Bittner, E. R. *J. Chem. Phys.* **2008**, *128*, 035101.
(25) Surjan, P. R. *Chem. Phys. Lett.* **2007**, *439*, 393−394.
(26) Dunning, T. H. *J. Chem. Phys.* **1989**, *90*, 1007−1023.
(27) Lischka, H.; Shepard, R.; Brown, F. B.; Shavitt, I. *Int. J. Quantum Chem.* **1981**, *S15*, 91−100.
(28) Shepard, R.; Lischka, H.; Szalay, P. G.; Kovar, T.; Ernzerhof, M. *J. Chem. Phys.* **1992**, *96*, 2085−2098.
(29) Lischka, H.; Dallos, M.; Shepard, R. *Mol. Phys.* **2002**, *100*, 1647−1658.
(30) Lischka, H.; Dallos, M.; Szalay, P. G.; Yarkony, D. R.; Shepard, R. *J. Chem. Phys.* **2004**, *120*, 7322−7329.
(31) Muller, T. *J. Phys. Chem. A* **2009**, *113*, 12729−12740.

(32) Lischka, H.; Shepard, R.; Shavitt, I.; Pitzer, R. M.; Dallos, M.; Mueller, T.; Szalay, P. G.; Brown, F. B.; Ahlrichs, R.; Boehm, H. J.; Chang, A.; Comeau, D. C.; Gdanitz, R.; Dachsel, H.; Ehrhardt, C.; Ernzerhof, M.; Hoechtl, P.; Irle, S.; Kedziora, G.; Kovar, T.; Parasuk, V.; Pepper, M. J. M.; Scharf, P.; Schiffer, H.; Schindler, M.; Schueler, M.; Seth, M.; Stahlberg, E. A.; Zhao, J.-G.; Yabushita, S.; Zhang, Z.; Barbatti, M.; Matsika, S.; Schuurmann, M.; Yarkony, D. R.; Brozell, S. R.; Beck, E. V.; Blaudeau, J.-P.; Ruckenbauer, M.; Sellner, B.; Plasser, F.; Szymczak, J. J. COLUMBUS, an Ab Initio Electronic Structure Program, release 7.0, 2011. www.univie.ac.at/columbus (accessed Dec 1, 2011).
(33) Trofimov, A. B.; Schirmer, J. *J. Phys. B: At., Mol. Opt. Phys.* **1995**, *28*, 2299−2324.
(34) Weigend, F.; Haser, M.; Patzelt, H.; Ahlrichs, R. *Chem. Phys. Lett.* **1998**, *294*, 143−152.
(35) Hättig, C.; Weigend, F. *J. Chem. Phys.* **2000**, *113*, 5154−5161.
(36) Hättig, C.; Köhn, A. *J. Chem. Phys.* **2002**, *117*, 6939−6951.
(37) Hattig, C. *Adv. Quantum Chem.* **2005**, *50*, 37−60.
(38) Schafer, A.; Horn, H.; Ahlrichs, R. *J. Chem. Phys.* **1992**, *97*, 2571−2577.
(39) Weigend, F.; Kohn, A.; Hattig, C. *J. Chem. Phys.* **2002**, *116*, 3175−3183.
(40) Plasser, F.; Lischka, H. *J. Chem. Phys.* **2011**, *134*, 034309.
(41) Karney, C. F. F. *J. Mol. Graphics Modell.* **2007**, *25*, 595−604.
(42) Ponder, J. W.; Richards, F. M. *J. Comput. Chem.* **1987**, *8*, 1016−1024.
(43) Schafer, A.; Huber, C.; Ahlrichs, R. *J. Chem. Phys.* **1994**, *100*, 5829−5835.
(44) Ahlrichs, R.; Bar, M.; Haser, M.; Horn, H.; Kolmel, C. *Chem. Phys. Lett.* **1989**, *162*, 165−169.
(45) Boys, S. F.; Bernardi, F. *Mol. Phys.* **1970**, *19*, 553−566.
(46) Olaso-Gonzalez, G.; Merchan, M.; Serrano-Andres, L. *J. Am. Chem. Soc.* **2009**, *131*, 4368−4377.
(47) Schaftenaar, G.; Noordik, J. H. *J. Comput.-Aided Mol. Des.* **2000**, *14*, 123−134.
(48) Shepard, R. In *Modern Electronic Structure Theory*; Yarkony, D. R., Ed.; World Scientific: Singapore, 1995; pp 345−458.
(49) *Mathematica*, version 5.2; Wolfram Research, Inc.: Champaign, IL, 2005.
(50) Jones, E.; Oliphant, T.; Peterson, P.; et al. SciPy: Open Source Scientific Tools for Python, 2001. http://www.scipy.org/Citing_SciPy (accessed June 1, 2011).
(51) Jmol: An Open-Source Java Viewer for Chemical Structures in 3D. http://www.jmol.org/ (accessed March 1, 2012).
(52) Plasser, F. Wave Function Analysis Tools: Computational Tools for Analyzing Molecular Orbitals and Electronic Wavefunctions, 2012. http://homepage.univie.ac.at/felix.plasser/download.html (accessed March 1, 2012).
(53) Ammeter, J. H.; Buergi, H. B.; Thibeault, J. C.; Hoffmann, R. *J. Am. Chem. Soc.* **1978**, *100*, 3686−3692.
(54) Tsuzuki, S.; Honda, K.; Uchimaru, T.; Mikami, M. *J. Chem. Phys.* **2004**, *120*, 647−659.
(55) Das, A.; Mahato, K. K.; Chakraborty, T. *J. Chem. Phys.* **2001**, *114*, 6107−6111.
(56) Nachtigallova, D.; Hobza, P.; Ritze, H. *Phys. Chem. Chem. Phys.* **2008**, *10*, 5689−5697.
(57) Perun, S.; Sobolewski, A. L.; Domcke, W. *J. Am. Chem. Soc.* **2005**, *127*, 6257−6265.
(58) Plasser, F.; Aquino, A. J. A.; Lischka, H. *J. Phys. Chem. A*, accepted for publication; DOI: 10.1021/jp304725r.
(59) Shang, Y.; Li, Q.; Meng, L.; Wang, D.; Shuai, Z. *Theor. Chem. Acc.* **2011**, *129*, 291−301.
(60) Panda, A.; Burghardt, I.; Plasser, F.; Aquino, A. J. A.; Lischka, H. Manuscript to be submitted for publication.
(61) Kirova, N. *Polym. Int.* **2008**, *57*, 678−688.